



Full Length Article

Distinguishing the glass, crystal, and quasi-liquid layer in 1-methylnaphthalene by using fluorescence signatures

Jan Zezula^a, David Mužík^a, Johannes Bachler^b, Thomas Loerting^b, Dominik Heger^{a,*}^a Department of Chemistry, Faculty of Science, Masaryk University, Kamenice 5, 625 00, Brno, Czech Republic^b Institute of Physical Chemistry, University of Innsbruck, Innrain 52c, A-6020, Innsbruck, Austria

ARTICLE INFO

Keywords:

Condensed phases
Luminescence
Surface premelting
Quasi-liquid layer
Cold crystallization
Excimers

ABSTRACT

The fluorescence of crystalline 1-methylnaphthalene is monomer-like, while liquid and glass exhibit excimeric emissions. We detail the temperature dependence of the fluorescence emission and excitation spectra in the range of between 77 K and 295 K. These spectra provide exhaustive information about the state and temperature of 1-methylnaphthalene. The glass, formed by abrupt quenching in liquid nitrogen or methane, devitrifies at (155 ± 5) K, and the liquid then undergoes cold crystallization at around 170 K. In 1-methylnaphthalene crystals, an excimeric emission appears at approximately 40 K below the melting point, a process we ascribe to the formation of dimers due to surface premelting; such a quasi-liquid layer exists at the surface well below the freezing point, remaining uncrystallized. The premelted layer is clearly distinguishable from the bulk glass via fluorescence spectroscopy, which facilitates state identification.

1. Introduction

Crystalline and vitrified states differ in numerous properties [1–6], such as the mechanical behavior [7], expansivity [8–11], elasticity [10, 12], diffusion coefficients [13], thermal conductivity [14–18], Young module [10], vapor pressure above the sample [19], luminescence [20], X-ray and neutron diffraction [20,21], and chemical reactivity [4,22]. The decision on whether any given compound will crystallize or vitrify when cooled down from its liquid phase depends on the time allowed for the solidification [7,22,23]. The crystallized phase can be distinguished from the vitrified state via a number of methods, including Raman, IR, X-ray, neutron diffraction, dielectric relaxation spectroscopies [24] and calorimetry [25–27]. Calorimetry is a convenient method to observe the heat capacity changes that accompany many physical processes within matter; therefore, this approach facilitates observing the glass transition and crystallization of bulk matter. We attempted to apply the technique to the study of freeze-concentrated solutions (FCS) in polycrystalline ice matrix; however, the observation sensitivity limits were encountered [28]. The FCS is a state into which most solutes pass after the freezing of an aqueous solution; such a state is thus very relevant in industrial, laboratory, and natural freezing [1,29]. The physical states of the compounds that have aggregated between the ice crystals were, therefore, advantageously followed by synchrotron X-ray diffraction [30],

and, in terms of spectroscopy, by Raman [31], EPR [32], UV–Vis [33], IR [26], and fluorescence.

We previously employed UV–Vis absorption and fluorescence spectroscopies to characterize the FCSs as regards substantial compounds aggregation and acidity changes [34–37]. Recently, the fluorescence of naphthalene facilitated distinguishing spectroscopically more subtle details of the FCS, namely, the crystallization and glass formation in frozen aqueous solutions [28,38–40]. Furthermore, the plasticity of the amorphous state was revealed when, unlike slow freezing, fast freezing allowed a sufficient amount of water in the FCS [28]. The advantages of the fluorescence method include its low detection limits and the fact that the technique has zero background signal [41].

We attempted to apply the fluorescence spectroscopy of 1-methylnaphthalene (MeNp) in examining frozen aqueous solutions [28], yet some of the compound's properties, e.g., the temperature-dependent position of the excimeric maximum, remained unexplained and prompted us to propose this follow-up study. MeNp possesses many properties that require the compound to be a good molecular probe in material studies. The pure MeNp is liquid at room temperature [28, 42–44]. At these conditions, MeNp exhibits emission spectra that consist of one main broad and unresolved band with a maximum at approximately 400 nm and a monomer-like emission at around 325 nm [28,42], whereas the broad 400 nm band was assigned to an excimer emission

* Corresponding author.

E-mail address: hegerd@chemi.muni.cz (D. Heger).<https://doi.org/10.1016/j.jlumin.2023.119917>

Received 3 March 2023; Received in revised form 18 April 2023; Accepted 10 May 2023

Available online 11 May 2023

0022-2313/© 2023 Elsevier B.V. All rights reserved.

[42].

In order to understand the MeNp spectroscopy in frozen aqueous solutions, we took a step back to examine in detail the fluorescence emission and excitation spectra of pure MeNp; these spectra allow an unambiguous identification of the liquid, crystallized, and amorphous phases at sample temperatures between 77 K and 295 K.

2. Experimental part

The liquid MeNp was purchased from Alfa Aesar (96%) and Supelco (analytical standard) and used as received. Aliquots of the pure liquid MeNp were frozen using two methods, namely, fast and slow cooling. In the fast-cooled samples, the quartz capillary (inner diameter ~ 0.1 cm) with the MeNp at room temperature (295 K) was immersed in liquid methane ($T_b = 91$ K) or liquid nitrogen ($T_b = 77$ K), both at $T = 77$ K, as specified for each experiment. In such freezing, the average cooling rate from 295 K was estimated to be 50 K s^{-1} and $(5.6 \pm 0.1) \text{ K s}^{-1}$, respectively [28]. After the freezing, each sample was inserted into an optical cryostat precooled to 77 K. The slow cooling was performed in an Optistat DN2 cryostat (Edinburgh Instruments) using a cooling gradient of $2 \text{ K min}^{-1} \approx 0.033 \text{ K s}^{-1}$.

The fluorescence emission and excitation spectra were recorded by means of an FLS 920 fluorescence spectrometer (Edinburgh Instruments) equipped with a 450 W Xe lamp as a light source, a PMT detector, double grating monochromators, and polarization filters that had been set to 0° and 90° for the excitation and detection, respectively.

The measurements were performed under front-face geometry, utilizing an Optistat DN2 cryostat (Oxford Instruments) within the indicated range of temperatures. After reaching the set temperature, the samples were kept at that level for 20 min prior to the fluorescent measurement.

The used excitation and detection wavelengths of the fluorescence spectra are indicated by λ_{exc} and λ_{det} , respectively.

The derivatives of the fluorescence spectra were calculated to resolve the peak maxima. A step-by-step filter-based program was applied to calculate the derivative curves [45,46]. The averages were calculated from maxima that had been determined by using the first to the eighth derivations. An MeNp solution in cyclohexane was prepared by dissolving a certain amount of MeNp in 25 mL of cyclohexane (VWR Spectronorm, $\geq 99.7\%$). The UV-vis spectra were recorded with a Cary 5000 UV-vis spectrophotometer, utilizing a quartz cuvette. Pure solvent spectra were used for the baseline correction.

The differential scanning calorimetry (DSC) measurements were carried out on a DSC 8000 by PerkinElmer that was calibrated using indium, adamantane and cyclopentane for a heating rate of 30 K min^{-1} . Pure MeNp was vitrified by placing a small droplet (ca $8 \mu\text{L}$) on a steel surface precooled with liquid nitrogen. The transparent product was transferred into an aluminum crucible and cold-loaded into the instrument. Calorimetric traces were recorded between 93 K and 298 K with heating/cooling rates of 30 K min^{-1} . A second heating scan served as a baseline.

The powder diffraction was executed *in situ* at an ambient pressure on a D8 Bruker Advance X-ray diffractometer equipped with a low-temperature Oxford chamber. A two-stage helium cryostat allowed scans to be performed between 80 K and 210 K. The X-ray source with the incident wavelength of $\lambda = 1.54178 \text{ \AA}$ (CuK α) and the detector were set up in a 2θ geometry. A Goebel mirror prevented distortion of the Bragg reflections. A volume of $40 \mu\text{l}$ of the sample, quenched in liquid nitrogen and then powdered, was transferred onto a sample holder made of nickel-plated copper precooled to approximately 80 K. The chamber was evacuated, and diffractograms were recorded in steps upon heating, with the individual temperatures reaching 6 K min^{-1} ; each scan took about 20 min. The step-like temperature profile involving slow heating rates led to slightly lower transition temperatures, typically ca. 10–20 K lower compared to the linear ramps at the high rates employed in calorimetry [47].

3. Results

3.1. Fluorescence spectra of the liquid, crystals, and glass

The fluorescence spectra of the liquid MeNp at RT and the spectra at 77 K after slow and fast cooling are presented in Fig. 1. The fluorescence emission spectrum of the liquid at 295 K (shown in Fig. 1, A) consists of a broad excimeric band (ranging from 315 nm to 530 nm, peaking at 387 nm) and a small monomer-like peak at 323 nm, in accordance with previous literature [28,42,48]. The emission of MeNp glass (fast-cooled in liquid methane) measured at 77 K is similar to the spectrum of the liquid MeNp at 295 K; only small monomer-like peaks at the blue edge of the spectrum are missing. By contrast, MeNp slow-cooled from 295 K to 77 K results in crystals which exhibit resolved bands in fluorescence emission at 319, 325, 329, 334, 339, 345, 351, 356, 363, 372, 383, and 392 nm (red line in Fig. 1), in agreement with the literature [28,49–51]. The spectra monitored in the cooling process are documented in Fig. S1 and Text S1, where in fluorescence the crystalline phase is very clearly distinguished from the liquid and the glassy states. The differences between the glass and the liquid are less pronounced. In fluorescence excitation there is a more pronounced distinction of the glass and the liquid.

The fluorescence excitation spectra of the liquid MeNp at 295 K are represented in Fig. 1, B. The excitation maxima revealed through derivation are at 250, 257, 265, 278, 291, 302, 307, 324, and 332 nm, while the last band is the most distinct one (listed in Table 1). The glass of MeNp at 77 K has excitation maxima revealed by derivation at 250, 259, 267, 281, 292, 302, 312, 318, and 324 nm. The most prominent feature to differentiate between the glass and the liquid is the shift of the sharp edge from 340 nm in the liquid to about 330 nm in the glass. The excitation spectrum of the MeNp crystals at 77 K shows bands at 265, 273, 285, 296, 312, 317, and 321 nm, resembling the excitation spectrum of MeNp in the solutions (see the positions of the individual bands in Table S1).

To uncover the origin of the fluorescence excitation band at 332 nm in the liquid, we performed fluorescence emission measurements using excitation wavelengths that exceeded those of the monomer absorption; the applied excitation does not have sufficient energy to populate any excited state of the monomer. At 295 K, we were able to excite the liquid MeNp using light with a wavelength of up to 345 nm (Fig. S2) while still obtaining an excimer signal. The broad band with a maximum at 387 nm that corresponds to the excimer did not change its shape when a range of excitation wavelengths were applied. Concerning the MeNp crystals, the longest wavelength allowing us to discern the emission spectrum was 325 nm at 77 K (Fig. S3). The emission spectra of the MeNp glass were elicited by applying light with wavelengths as long as 335 nm at 77 K (Fig. S4).

3.2. Crystals

The MeNp crystals were heated from 77 K to 255 K, and their fluorescence emission and excitation spectra were monitored. The emission spectra of the crystals change in the heating process: the two bands at the lowest wavelengths (at 325 nm and 329 nm) diminish substantially when the sample is heated from 77 K to 170 K, whereas the other bands remain intact (Fig. 2, A). Upon heating the sample to 200 K, a broad band with a maximum around 400 nm becomes apparent (Fig. 2, A, green line) to substantially grow by isothermal annealing for 90 min (blue line). After further heating to 255 K, the MeNp becomes a liquid having a typical broad excimeric band with a maximum at 395 nm and a shoulder at around 325 nm (as described above).

The fluorescence excitation spectra are shown in Fig. 2, B. At 77 K (black line), there are resolved bands at 265, 273, 285, 296, 312, 317, and 321 nm (listed in Table 1). Upon heating (to 170 K and higher temperatures), the bands remain at the same positions except for the one at 321 nm, which is slightly bathochromically shifted with increasing

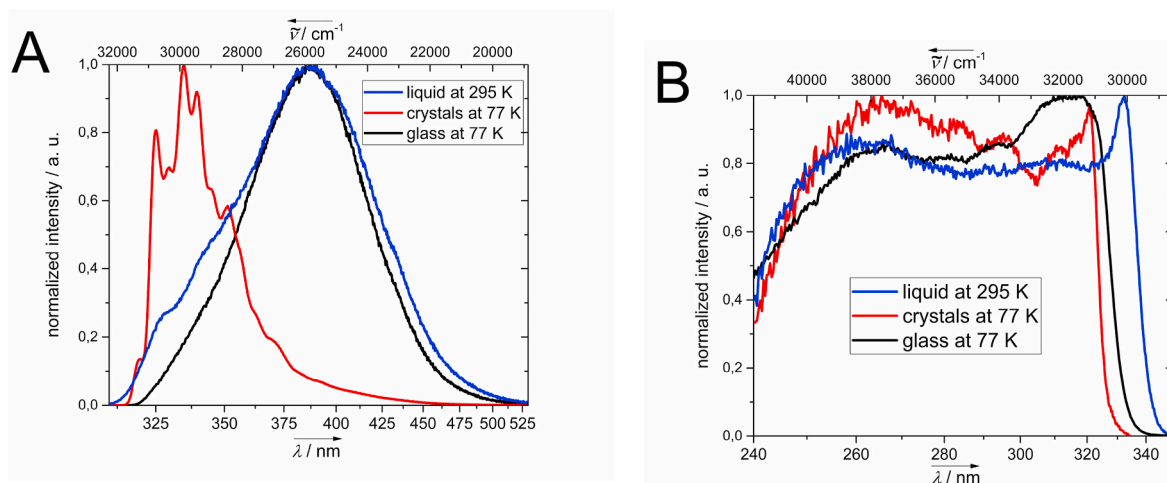


Fig. 1. The normalized fluorescence emission (A, $\lambda_{\text{exc}} = 274$ nm) and excitation (B, $\lambda_{\text{det}} = 390$ nm) spectra of the **liquid** MeNp at 295 K (blue), **crystals** formed by slow cooling (red), and **glass** resulting from fast cooling in liquid methane (black). The spectra of the crystals and glass were measured at 77 K.

Table 1

The excitation maxima determined by numerical derivatives of the liquid MeNp at 295 K, MeNp glass at 77 K, and MeNp crystals at 77 K.

MeNp	Excitation maximal λ / nm											
Liquid at 295 K	250	257	265	278	291	302	307				324	332
Glass at 77 K	250	259	267	281	292	302		312	318	324		
Crystals at 77 K			265	273	285	296		312	317	321		

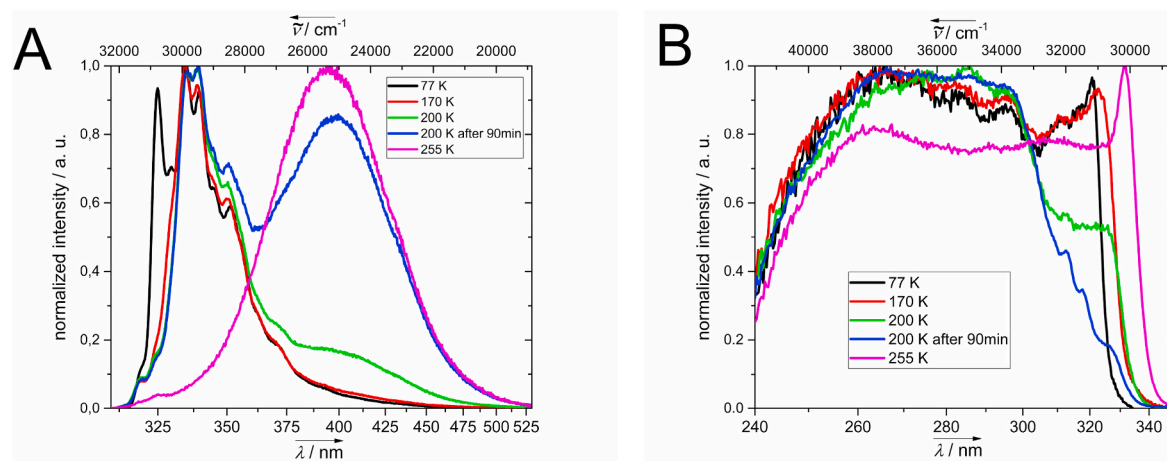


Fig. 2. The normalized fluorescence emission (A, $\lambda_{\text{exc}} = 274$ nm) and excitation (B, $\lambda_{\text{det}} = 390$ nm) spectra of the MeNp crystals at 77 K (black); the **crystals** were heated to 170 K (red), 200 K (green), and then 200 K after a 90-min delay (blue). Subsequently, we performed heating to **liquid** MeNp at 255 K (magenta).

temperature (323 nm at 170 K), ending at 326 nm at 200 K. The positions of all bands in the excitation spectra of the MeNp crystals at the indicated temperatures are given in Table S1. Moreover, besides the bathochromic shift of the band above 320 nm, the heating of the MeNp crystals to 200 K leads to a relative increase in the intensity of the excitation spectra at wavelengths below 300 nm (Fig. 2, B). The increase continues even when the sample is kept at 200 K for a prolonged time. The time evolution of the isothermal annealing experiment at 200 K is documented in Fig. S5 and Text S2, where the absolute detected light intensities are given. At 255 K, the MeNp is already liquid, with a typical excitation spectrum. Moreover, the crystals prepared by slow cooling from 295 K to 220 K were examined by using various excitation wavelengths (Fig. S6), and the proportion of intensities between the excimeric part and the monomeric one is shown in Fig. S7.

3.3. Glass

The MeNp fast cooled in liquid methane resulted in bulk glass. Arguments for the glassy character will be outlined below. The fluorescence emission and excitation of the MeNp glass was examined within the temperature range between 77 K and 170 K. At 77 K, there was an excimer fluorescence peaking at 387 nm. When heating the MeNp glass from 77 K to 150 K and 160 K, we observed a subtle difference in the excimer emission spectra in the wavelength range from 320 nm to 380 nm (the black and green lines in Fig. 3, A; for finer temperature steps see Fig. S8). The peak in the emission spectrum at 77 K rises more steeply than that at 160 K, which, despite starting in the same spectral region at 320 nm, has a more gradual increase. At the same time, the excimer maxima bathochromically shift from 387 nm at 77 K to 392 nm at 160 K. The positions of the excimer maxima at the indicated temperatures are

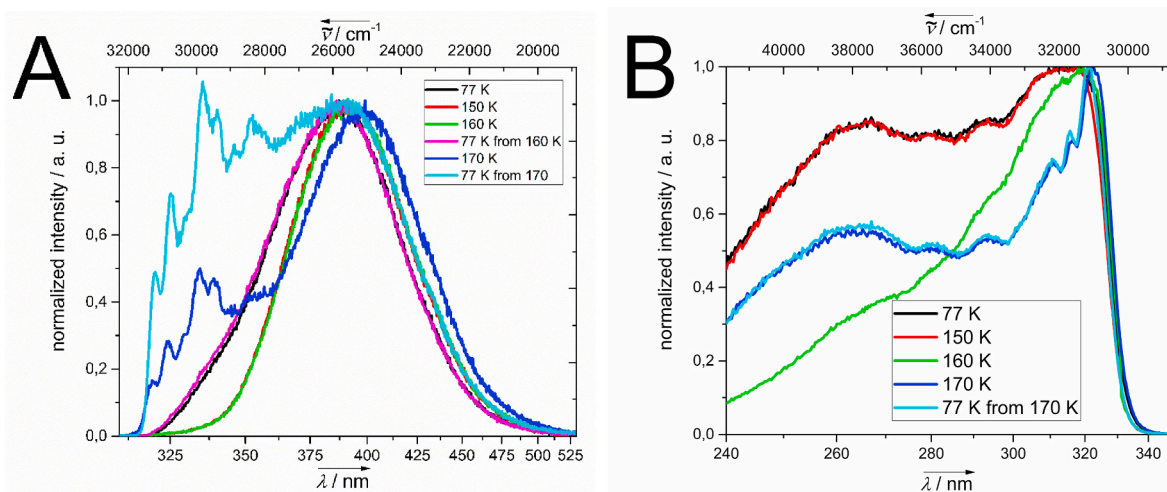


Fig. 3. The normalized fluorescence emission (A, $\lambda_{\text{exc}} = 274$ nm) and excitation (B, $\lambda_{\text{det}} = 390$ nm) spectra of an MeNp sample fast cooled to 77 K (black), heated to 150 K (red) and 160 K (green), cooled down to 77 K (magenta), heated to 170 K (blue), and finally cooled down to 77 K (cyan).

listed in Table S3 and plotted in Fig. 5 (red dots). After heating the MeNp sample to 160 K and cooling it down to 77 K, the emission spectrum returned close to its original 77 K position, including the maximum and the shape (Fig. 3, A, magenta line). The derivation of the spectra at 77 K and 100 K revealed the positions of the maxima of the individual constituting bands listed in Table S2 and B.

The temperature-induced changes were reversible below 160 K, as is evident from a comparison of the original spectra at 77 K with those at 77 K, where the sample had been cooled down from 160 K. Once the MeNp was heated to 170 K or beyond, the signals of the crystals appeared, and simultaneously the excimer maximum bathochromically shifted to 398 nm. While heating the MeNp glass, we observed visually that a white glassy substance cleared up to become liquid at around 160 K. At further heating to 170 K, small crystals were found, floating in the liquid MeNp. Cooling the partly crystallized glass down from 170 K to 77 K led to a hypsochromic shift of the excimer maxima to 387 nm and a relative increase of the intensity of the bands of the MeNp crystals with respect to the excimer part (the excimer maxima for the glass and partly crystallized glass are shown in Fig. 5 as red dots and blue triangles, respectively).

The fluorescence excitation spectra were recorded at 77, 150, 160, 170 and 77 K, as depicted in Fig. 3, B. The band maxima are given in Table S1. The spectrum at 150 K is almost identical in relative intensity and band position with the spectrum at 77 K. At 160 K, the shape of the spectrum is substantially different. The absolute intensity of the spectrum measured at 160 K is 1000 times higher than that of the spectrum at 150 K, keeping the same setting of the spectrometer. This abrupt increase in signal intensity was noted during three independent measurements. Nevertheless, the band maxima revealed by the numerical derivations are at positions resembling the spectrum at 77 K (Table S1 and C). At 170 K, the excitation spectrum changes again and maintains its shape when the sample is cooled down to 77 K. Even though the overall spectral shape seems altered compared to those at lower temperatures (especially at wavelengths above 300 nm, where the bands at 311, 317 and 322 nm become well-resolved), the derivation analysis shows that the positions of the bands remain nearly unaltered (Table S1 and C).

Furthermore, we performed another experiment to detail the crystallization of the MeNp glass; the process was slow enough to be monitored in the emission spectra for 220 min (Fig. S9). The MeNp glass was heated from 77 K to 180 K, and its fluorescence emission was monitored immediately after reaching 180 K, at 20, 30, 40, 70, 120, and 220 min into the process. A decrease in the intensity of the excimer (elicited from the glass, $\lambda_{\text{max}} = 399$ nm) at the expense of the monomer

(due to the MeNp crystals) with increasing time is evident from the spectra. Moreover, the partly crystallized glass sample was examined using a range of excitation wavelengths (Fig. S10). We were able to use an excitation wavelength as high as 335 nm, obtaining an excimer emission.

The DSC thermogram of the MeNp glass (fast cooled) was measured at temperatures between 140 K and 200 K with the heating rate of 30 K min^{-1} (Fig. 4). The most important features in the thermogram consist of the devitrification endotherm of glass at $T_{g,\text{Onset}} = 168 \text{ K}$ and the crystallization exotherm commencing at T_x ca 183 K. The difference in heat capacity between the glass and the liquid of MeNp amounts to $66.5 \text{ J K}^{-1} \text{ mol}^{-1}$.

3.4. Excimer maxima

The excimer maxima of the MeNp are plotted as a function of temperature (ranging within 77–295 K) in Fig. 5; various species are responsible for the emission under these conditions, namely, glass, crystals, and liquid. The glassy MeNp (red dots) at 77 K has an excimer maximum at 387 nm. Upon heating, the bathochromic shift was

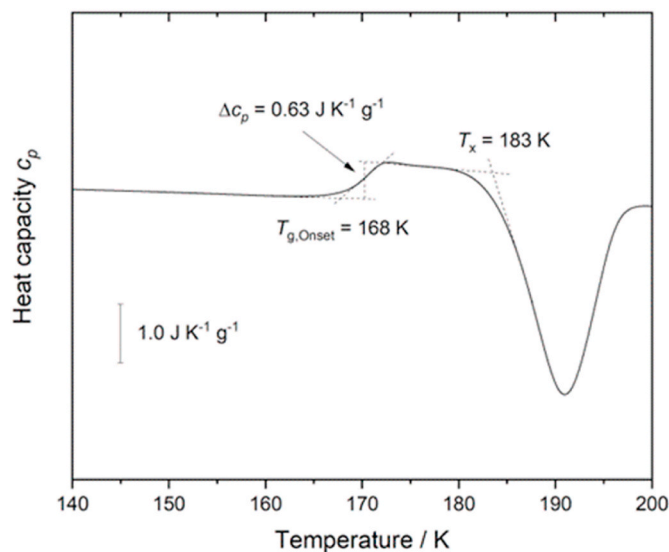


Fig. 4. A differential scanning thermogram of the MeNp glass: heating at the rate of 30 K min^{-1} .

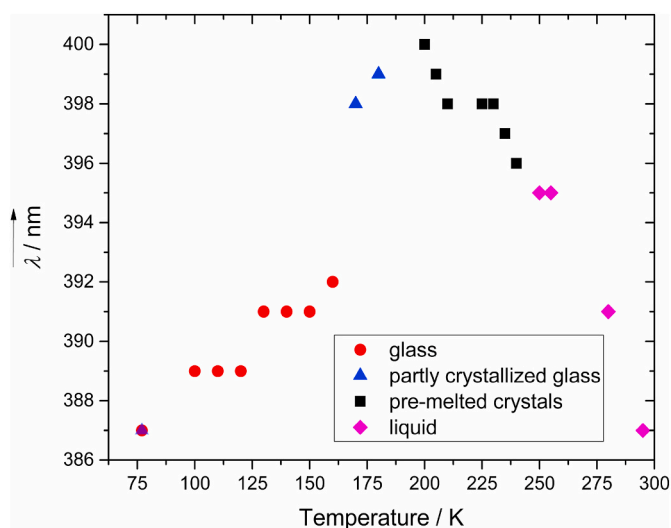


Fig. 5. The temperature dependence of the excimer maximum wavelength in the pure MeNp: the glass (red dots), glass partly crystallized at 170 K and cooled down to 77 K (blue triangles), pre-melted crystals (black squares), and liquid MeNp (magenta diamonds).

observed to reach 392 nm at 160 K. Where the MeNp glass partly crystallized, the excimer maxima shifted substantially to 398 nm and 399 nm (blue triangles), as observed at 170 K and 180 K, respectively. When the partly crystallized glass was cooled back down to 77 K, the maximum returned to its previous position at 387 nm. Upon heating the crystals from 77 K to 200 K, the excimeric signal with a maximum at 400 nm appeared in the fluorescence emission spectrum. Heating the sample to higher temperatures led to the hypsochromic shift of the maximum reaching 396 nm at 240 K. At 250 K, the MeNp was liquid, with an excimer maximum at 395 nm (magenta diamonds); its further heating caused the hypsochromic shift to reach 387 nm at 295 K.

3.5. XRD

The X-ray diffractograms of the MeNp (ca. 40 μ l) fast cooled in liquid nitrogen were recorded at 77 K and after gradual heating to 150 K, 190 K, and 210 K; this stage was followed by cooling down to 190 K and 80 K (Fig. 6, Fig. S11). Furthermore, the liquid sample was measured at 260

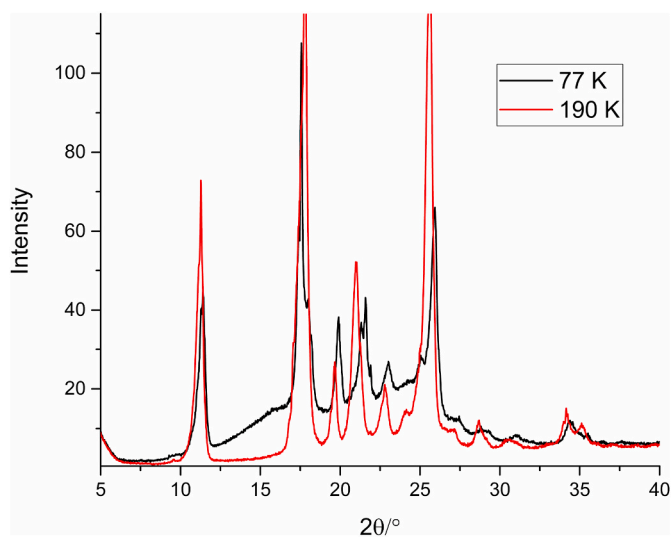


Fig. 6. The X-ray diffractograms of the MeNp fast cooled in liquid nitrogen, measured at 77 K (black) and after heating to 190 K (red).

K, with the broad peak having a maximum at 24° (2θ). The Bragg diffraction maxima are listed in Table S4. At 77 K and 150 K, the MeNp exhibits sharp Bragg peak characteristics in the MeNp crystals and a broad halo band in the amorphous MeNp (within the range of 2θ from 11° to 30°). Once the sample was heated to 190 K, the halo disappeared and was not present either after the heating of the sample to 210 K or during the subsequent cooling. The subtraction of the diffractograms before and after the heating, at 77 K and 80 K, respectively (Fig. S12), revealed the approximate position of the broad band due to the amorphous glass at ca. 20° (2θ).

4. Discussion

4.1. Liquid

The fluorescence emission and excitation spectra can be applied to distinguish the (supercooled) liquid, crystalline, and glassy states of MeNp.

The emission spectra of the liquid (Fig. 1, A, blue, at 295 K; Fig. 2, A, magenta at 255 K) are dominated by an excimeric signal having a maximum around 390 nm and supplemented with a small monomer-like emission band at 323 nm, which is well discernible above the noise, especially at higher temperatures. The relative growth in the intensity of the monomer-like emission with rising temperature was reported in the literature [48]. The excimer maximum shifts hypsochromically with rising temperature (Fig. 5), and this fact corresponds to an increasing extent of the monomeric emission at higher temperatures. The excitation spectrum of the liquid MeNp has not been published thus far, to the best of our knowledge. Interestingly, the excitation spectrum extends up to 345 nm, i.e., to wavelengths longer than the 0-0 transition of a single solvated molecule (Fig. 1, B, Fig. S1 and B, and Fig. S2), and exhibits a sharp maximum at around 332 nm (at 295 K) and two broad maxima at 307 nm and 265 nm. The shift of the excitation spectrum's edge informs us quantitatively about the change in the lowest possible energy that still leads to populating the excited state. Here, we determine the edge as the half height of the most red-shifted band in the excitation spectrum. The liquid MeNp edge position at 295 K is shifted by ca. 17 nm bathochromically compared to a diluted MeNp cyclohexane solution (Fig. 10 and Fig. S1 and B). This fact suggests the importance of the ground state interactions in the liquid MeNp, these interactions being probably caused by dimer formation. A bathochromic shift in the dimer absorption spectra was suggested for naphthalene already previously [52]. The X-ray diffraction patterns of liquid MeNp at 293 K were interpreted in terms of short-range ordering due to formation of parallel displaced dimers, where the dipoles of the molecules are arranged in an antiparallel orientation [53]. Conceivably, these orientations result in excimers after excitation. Similarly, parallel-displaced structures were proposed by simulations to be more stable than T-shaped orientations in the gas phase concerning MeNp [51]. The parallel-displaced dimers suggested for liquid MeNp by Drozdowski [53] stand in contrast to the arrangement in liquid benzene where Y-shaped dimers prevail [54]. However, in benzene the parallel displaced arrangement still represents a minor population and is the ground state arrangement that enables an instantaneous formation of an excimer [54,55].

4.2. Crystals

The crystals at 77 K absorb at wavelengths only below 325 nm, and their emission results solely in a monomer signal (Fig. S3). However, the absorption edge shifts bathochromically with increasing temperature, as detailed in Fig. 2, B. The shift is reproducible and does not show thermal hysteresis. As a matter of fact, this absorption shift can explain the apparent changes in the emission spectra at the same conditions. The normalized excitation and emission spectra are represented in Fig. 7, which shows distortions of the spectra at the low wavelength region (mainly the emission bands at 325 nm and 329 nm exhibit reduced

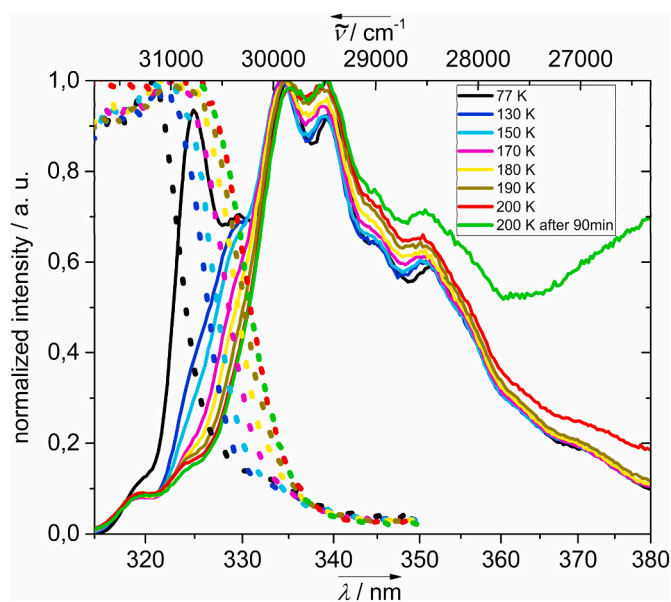


Fig. 7. A detail of the region from 310 nm to 380 nm of the fluorescence excitation spectra ($\lambda_{\text{det}} = 390$ nm, dotted lines) normalized to a local maximum, together with the normalized fluorescence emission spectra ($\lambda_{\text{exc}} = 274$ nm, full lines) of the MeNp crystals at 77 K (black), which were heated to 130 K (blue), 150 K (cyan), 170 K (magenta), 180 K (yellow), 190 K (dark yellow), and 200 K (red); represented is also the situation at 200 K after a 90-min delay (green).

intensities) through self-absorption and, even more so, with increasing temperature. A similar observation was made for naphthalene crystals [28,40]. No excitation edge change caused by keeping the sample at 200 K was observed, despite the larger increase in the excimer signal. We interpret this observation in terms of a temperature-enhanced vibrational excitation of the MeNp crystals.

Another notable change in the emission spectra that relates to rising temperature is the gradual increase of the excimer signal. A small but systematic growth of the signal can be seen at temperatures as low as 170 K (410 nm, Fig. 2, A), gaining momentum above 180 K. Apparently, the relative intensity of the crystal signal abates, and a new species with emission maxima at 400 nm intensifies. The progressive change is also discernible through examining the excitation spectra (Fig. 2, B), where an increased signal intensity is observed below 320 nm (relative to the signal above this threshold; note that the displayed spectra are normalized). Even though the signal above 320 nm exhibits a relative loss in intensity, it shifts bathochromically, as detailed in Fig. 7. A raw quantification of the process is shown in Fig. S13, where the ratio of the excitation intensities at 320/273 nm (for detection at 390 nm) is plotted. The 320 nm value denotes the crystal absorption, whereas that of 273 nm corresponds mostly to the species appearing with increased temperature. It is demonstrated that the high temperature species starts to contribute to the signal at temperatures above 180 K. The appearance of the new species is not only temperature-dependent but also slow enough to be observed on the scale of minutes (Fig. S5).

The excitation spectrum at 200 K is subtracted from that at the same temperature, the latter being measured after 90 min (The original spectra are taken from Fig. S5); all of the curves are shown in Fig. 8, the orange one referring to the subtraction. Even though the subtraction is not perfect, and the resulting spectrum cannot be regarded as representing the pure species, the trend is revealed well: The spectrum due to the crystal absorption above 320 nm subtracts perfectly, and the remaining spectrum typical of the excimer appears more clearly, possessing the characteristic MeNp S0–S1 vibrational progression (313 nm and 318 nm) and two broad bands (266 nm and 300 nm). Furthermore, the obtained excitation spectrum resembles, to an extent, that of the liquid MeNp at 250 K (Fig. 8, blue; the individual bands are listed in

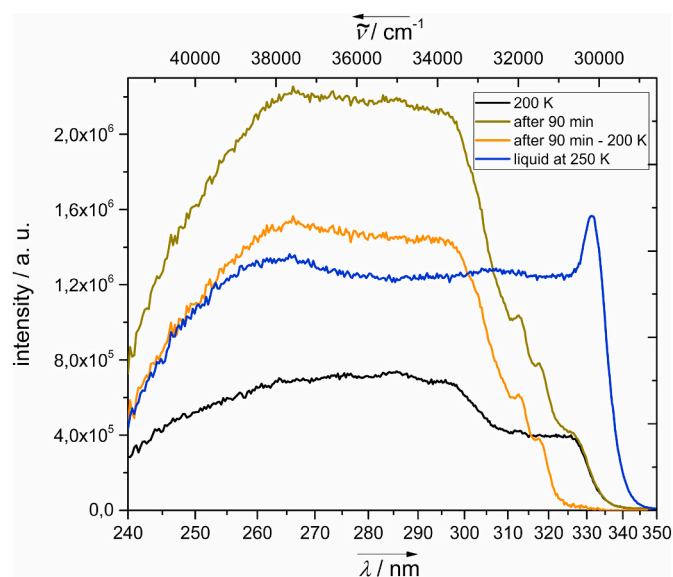


Fig. 8. The fluorescence excitation spectra ($\lambda_{\text{det}} = 390$ nm) of the MeNp crystals at 200 K, prepared by slow cooling of the MeNp to 77 K and subsequent warming, measured immediately after reaching the temperature of 200 K (black) and then after 90 min (dark yellow); the curves are completed with the subtraction of the first spectrum from the final one after 90 min (orange). The indications are supplemented with the fluorescence excitation spectra ($\lambda_{\text{det}} = 390$ nm) of the liquid MeNp at 250 K (blue).

Table S1). This is true especially of the broad band around 266 nm, where both these spectra overlap in a strikingly similar manner.

Based on the arguments of the temperature dependence, slow pace of the process, and similarity of the spectra to those of the liquid MeNp, we propose that the observed phenomenon is the formation of a quasi-liquid layer (QLL) on the crystal surfaces, also known as surface premelting [56–58]. The liberation of the surface molecules from the crystal lattice [59] allows their orientational relaxation, facilitating the excimeric emission. In the case of H₂O-ice, the QLL is present well below the T_m , which leads to effects such as regelation, electrification, and surface slipperiness of the ice, as first noticed by Faraday [60]. Depending on the sensitivity of the method employed, the onset temperature can be 40 K below the T_m or even only 1 K [2]. The presence of small amounts of impurities brings this onset temperature down to ca. 85 K below the T_m [61]. The QLL on the surface of Pb(110) was observed at 40 K below its melting point [62]; in Ar and Ne films, the QLL was detected at the lowest temperature of $0.8 \times T_m$ [63]. Considering the T_m of MeNp at approximately 240 K, such an estimate would predict the QLL at around 190 K, in agreement with our observations (180 K). However, the species present in the QLL does not match that in the liquid. This fact can be inferred from the significant differences in the excitation spectra (which miss most of the absorption above 300 nm, including the 332 nm peak in the QLL as compared to the liquid phase). The variance in the excitation spectrum was confirmed by the inability to elicit the excimeric emissions with an excitation light higher than 317 nm (Fig. S6), contradicting the ability to obtain the emission signal from the liquid and the glass through light with wavelengths as long as 345 and 335 nm, respectively (Fig. S2 and Fig. S4). The excitation spectral edge of the crystals is shifted bathochromically only by 3 nm as compared to the 10^{-4} M solution in cyclohexane; refer to Fig. 10 and Fig. S1 and B.

We tentatively propose interpreting the excimers within the QLL in terms of dimer formation. Certainly, other methods would be needed to deliver an unambiguous proof. The spectral differences between the aggregates (dimers) present in the QLL on the crystals' surface and the actual crystals are demonstrable via the selective excitation of the crystals in the presence of the QLL. Such a situation materializes at 220 K. The excitation-dependent emission spectra are represented in Fig. S6.

The two species can be identified in the emission: One from the crystals, which are selectively excitable above 320 nm and produce a monomeric emission, and the other from the dimer, which results in the excimer signal. Moreover, the intensity of the excimer emission signal, relative to that of the monomer (Fig. S6), follows the excitation spectrum of the QLL dimer (Fig. 8); this is exposed through the proportion of the wavelengths of 398 nm and 335 nm, Fig. S7.

Interestingly, the edge of the excitation band is not shifted bathochromically by the increased extent of the surface premelting at 200 K after a prolonged time. The situation is well recorded in Fig. S5 and B, where, despite the 5-fold increase in the emission intensity at wavelengths below 300 nm, the edge position does not alter. The temperature-induced bathochromic shift of the excitation edge might suggest that the observation arose from aggregation (dimerization); however, this is not the case. The ground state dimer is formed in the QLL, but its absorption does not exceed 317 nm (Fig. 8 and Fig. S6). Thus, the bathochromic shift of the excitation spectra must be associated with the absorption of the bulk crystals (not the QLL) and is likely caused by the vibration modes allowed at higher temperatures. The positions of the absorption edges are determined solely by the state of the MeNp (crystal, glass, or liquid) and the temperature. The dimeric species whose excitation results in an excimeric emission in the QLL do not reach the longest wavelengths (Fig. 8, orange).

We estimate the depth of the light penetration into the MeNp crystals to be below 800 nm for the 274 nm excitation and below 38 μm at 317 nm, based on the Lambert-Beer law and the density of liquid MeNp ($D = 1.001 \text{ g mol}^{-1}$, $A = 4$, $\epsilon(273 \text{ nm}) = 7000 \text{ dm}^3 \text{ mol}^{-1} \text{ cm}^{-1}$, $\epsilon(317 \text{ nm}) = 150 \text{ dm}^3 \text{ mol}^{-1} \text{ cm}^{-1}$). In cases where an emission of both the crystals and the QLL is observable (Fig. S5 and A and Fig. S6), we can estimate the relative abundances in the probed volume. The lesser excimer signal for the 317 nm excitation as compared to the 274 nm one (Fig. S6) is explainable by a smaller QLL proportion in the probed volume. Nonetheless, an excitation above 320 nm yields solely an emission of crystals in accordance with the subtraction spectra in Fig. 8, indicating that the species in the QLL do not absorb significantly but not that their contribution is too small due to a larger penetration depth.

No crystal structure of MeNp has been reported to date, to the best of our knowledge; we found only one article reporting the X-ray diffraction pattern [64]. Nonetheless, the MeNp crystal structure supposedly resembles that of naphthalene crystals, which are well documented [65]. In these crystals, the individual naphthalene molecules are arranged in perpendicular pairs of nearest neighbours, and therefore the fluorescence emission spectrum is of the monomer type and does not exhibit an excimeric emission. As an MeNp crystal results in the same monomer-like character of the spectra, we can expect a similar crystal arrangement. Conversely, the 1,3- and 1,4-dichloronaphthalenes crystal packing structure produces an orientation allowing excimers [66].

We have assigned the excimeric signals observed in the crystals above 180 K to the QLL. This fact appears to embody the most likely explanation, considering all of the experimental findings, the wavelength-dependent penetration depth in particular. We prefer this scenario over the other feasible option, namely, transformation between two crystal structures, as reported previously in the case of 2-methylnaphthalene [67]. For a definitive proof, a surface-sensitive structural technique, such as low-energy electron diffraction (LEED), would be required.

4.3. Glass

Formerly, the excimeric emission arising from liquid nitrogen-cooled MeNp samples with an emission maximum at 387 nm was interpreted as the luminescence from crystal defects [50]. By contrast, we argue herein that the excimeric emission from the quenched MeNp liquid arises from the glass; this fact is confirmed by DSC and X-ray diffraction.

Immersing a small volume (ca. 40 μl) of MeNp in liquid methane at 77 K yields an excimeric emission spectrum, i.e., an output very different

from that of the slowly frozen sample (Fig. 1, A). While the fast cooling in liquid methane (approx. cooling rate 50 K s^{-1}) produces solely an excimer emission (Fig. 1, A), the slower cooling in liquid nitrogen (approx. cooling rate 5.5 K s^{-1}) results in either samples exhibiting a pure excimer emission or those which, besides a broad emission of the excimer, contain resolved bands of MeNp crystals [28]. Apparently, during the latter cooling cycle the MeNp cannot fully vitrify, crystallizing partially. The (partial) crystallization typically accompanies slow cooling [27]. We established that the sample size plays a role in the vitrification process: The larger MeNp volumes applied in our previous experiments have a stronger tendency to crystallize [28]. In the referenced article, thicker quartz test tubes were used (an inner diameter of 0.6 cm) together with liquid nitrogen cooling, invariably delivering glass contaminated with MeNp crystals. The reason for the cooling rate in liquid nitrogen being slower than that in liquid methane is the Leidenfrost effect, where the boiling of liquid nitrogen produces a vapor layer slowing down the cooling [68–70]. It should be noted that the MeNp used in the above-referenced article [28] contained some fluorescing impurities (having signals above 400 nm). In the current study, by contrast, we used a purer MeNp, which does not show impurity signals. The MeNp contamination is a common problem which reflects in a range of reported melting points (235.8–242 K) [28,43,44].

Pure and crystal-contaminated MeNp glasses exhibit between 77 K and 150 K a reversible behavior without notable hysteresis (Fig. 3, A). We suggest that the temperature dependence of the emission spectrum cannot be explained by the altered ground state interaction alone: Rather, we interpret the changes in the shapes and positions of the emission spectra as following from the excited state stabilization. Already at 85 K, the glass appears to be plastic enough to allow some relaxation, resulting in spectral emission changes and a bathochromic shift of the excimeric emission maximum (Fig. S8). The excitation spectra, however, remain largely unaltered (Fig. 9). The bathochromic shift of the edge of the excitation spectrum is merely ca. 2 nm between 77 K and 170 K (Fig. 3, B), being too small to explain the abrupt emission changes, especially in the range from 77 K to 100 K. Simultaneously, the emission maximum exhibits a substantial bathochromic shift with increasing temperature (by more than 10 nm; Fig. 5 and Table S3). Considering both the excitation and the emission spectra (Fig. 9), we

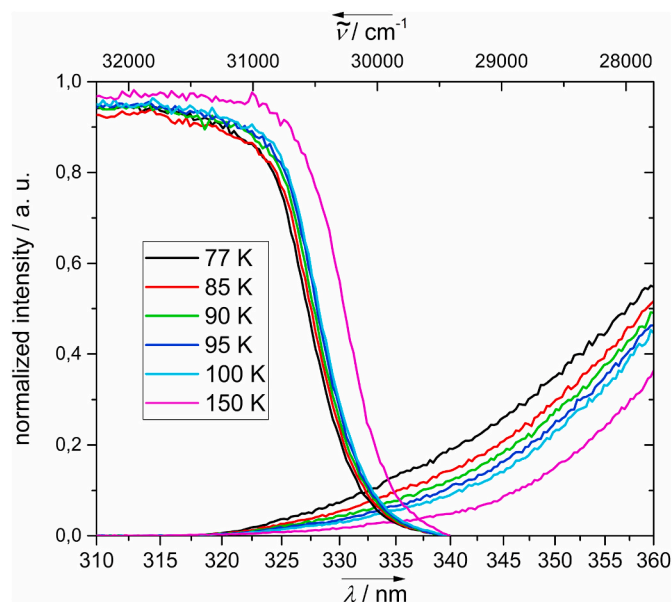


Fig. 9. A detail of the normalized fluorescence emission spectra region from 310 nm to 360 nm ($\lambda_{\text{exc}} = 274 \text{ nm}$, Fig. S8), plotted together with the normalized fluorescence excitation spectra ($\lambda_{\text{det}} = 390 \text{ nm}$) of the MeNp glass (prepared in liquid methane) at 77 K (black line) and at 85 K (red line), 90 K (green line), 95 K (blue line), 100 K (cyan line), and 150 K (magenta line).

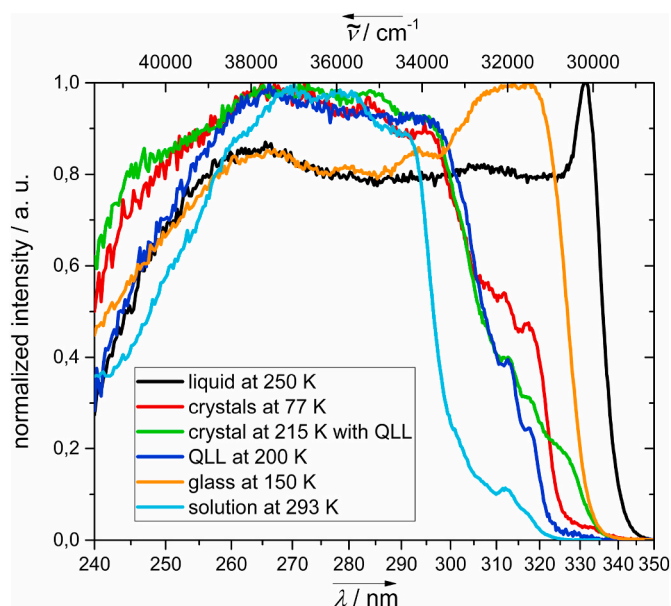


Fig. 10. The demonstrative fluorescence excitation spectra typical of the MeNp species, color-coded according to Scheme 1. All of the spectra were detected at ($\lambda_{\text{det}} = 390 \text{ nm}$) and are normalized, showing the liquid MeNp at 250 K (black), MeNp crystals at 77 K (red), crystals with the QLL at 215 K (light green), QLL gained via subtracting the spectrum that evolved during 90 min at 200 K (blue) from the zero time spectrum, glass (cooled in liquid methane) at 150 K (orange), and a 10^{-4} M MeNp solution in cyclohexane at 295 K (cyan).

conclude that the ground state interaction in the glass does not alter significantly below 150 K, whereas the excited state is allowed to relax more as the temperature rises. This behavior of the glass therefore contradicts that of the crystal (Fig. 7). We can only speculate if the emission signal around 340 nm that has been observed at 77 K to disappear upon higher temperatures is due to a particular frozen dimeric conformation which differs from the one responsible for the main emission band at 398 nm.

Heating the glasses turns them into a supercooled liquid above the glass transition temperature. Herein we observe a transformation into the liquid in samples cooled down rapidly in methane at 160 K and, regarding the more slowly cooled ones, in liquid nitrogen at 150 K. This information utilizes visual observation of the sample (the sample lost its opalescent appearance of the glass), together with an intensity increased ca. 1000 times and a shape distortion of the excitation spectra (Fig. 3, B, green). The higher glass transition temperature upon heating in the rapidly cooled samples agrees well with previously published expectations from other glasses. The rapidly cooled liquid diverges from the equilibrium at higher temperatures than the more slowly cooled one. Such glasses have higher fictive temperatures and excess entropy compared to the slow cooled ones [71–74]. We are presently unable to offer a certain explanation of the spectral changes; however, we propose a possible impact of the directional Mie scattering on the nucleated MeNp crystals, i.e., an effect potentially facilitating excitation of a larger number of molecules with detectable emission [75]. Another scenario lies in an increased fluorescence quantum yield in nucleated crystals [74]. The T_g onset value of the glass-to-liquid transition was found at 168 K via DSC (Fig. 4). The slightly higher value compared to the one found by fluorescence is caused by the higher applied rate of warming (30 K min^{-1}).

An irreversible cold crystallization (T_c) event is observed by fluorescence upon further heating between 160 K and 170 K (Fig. 3, A), the reason being a newly emerged emission of crystals in the spectra. In DSC the crystallization exotherm appears at ca 183 K (Fig. 4). At 180 K, the crystallization process is slow enough to be monitored through the emission spectra for 220 min (Fig. S9). A decrease in the intensity of the

excimer (which stands for an emission of the glassy MeNp) at the expense of the monomer (the MeNp crystals) with increasing time is evident from the spectra. Moreover, the excimeric emission maximum of the glass does not show any history dependence: Cooling the glass from 170 K to 77 K results in the same position of the maximum as in the glass formed from the liquid MeNp (Fig. 5).

By extension, a sample of partly crystallized glass was examined by using a range of excitation wavelengths (Fig. S10). An excitation wavelength as high as 335 nm is applicable, resulting in an excimer emission to prove the presence of uncrystallized glass. Another behaviour, contrasting to that of the crystals (Fig. S6), is the near absence of changes in the relative signal ratio for the crystal and the excimer. This indicates a homogeneous matrix where the penetration depth does not substantially affect the emission signal. The fact of MeNp crystallization is confirmed also by X-ray diffractograms (Fig. 6) as a halo peak disappearing after heating to 190 K. Interestingly, the same temperature was observed in relation to the disorder-to-order transition in the multilayers of MeNp deposited on the α -alumina surface [76], and the temperature of 185 K marked a transition between amorphous and crystalline naphthalene on the surfaces of ice [40] and gold [77].

4.4. Comparison

The glass differs from the liquid in not only the longest excitable wavelength (335 nm and 345 nm, respectively) but also in the X-ray diffraction pattern. The broad halo of the liquid MeNp peaks at 24° , whereas that of the glass does so at ca. 20° (Fig. S12). Similarly, the QLL is distinguished from the bulk glass in the inability to elicit excimeric emissions with an excitation light higher than 317 nm, contradicting the ability to obtain an excimeric signal from the glass by means of a light with a wavelength up to 335 nm (Fig. S4). The MeNp forms differ between each other in the excimeric emission maxima (Fig. 5); the excimer can be observed in the glass, QLL of the crystals, and liquid MeNp. The excimer maximum is characteristic of each medium and temperature: In the glass, it shifts from 387 nm at 77 K to 399 nm at 175 K; in the QLL on the surface, it decreases from 400 nm at 200 K to 396 nm at 240 K. The shift of the edge of the excitation spectrum of the crystal is much more pronounced than that of the glass, but both cases are bathochromic. These observations can be interpreted in terms of the stabilization of the ground and the excited states. In the glass, the ground state molecules do not alter their positions significantly, and only the excited state geometry relaxes, more markedly so at an increased temperature; thus, the emission maximum shifts to a longer wavelength. Conversely, in the QLL and the liquid, both the ground and the excited state relaxations are easily accomplished, resulting in a hypsochromic shift of the excimeric emission maximum.

The above-outlined details of the spectral behavior allow us to assign the individual material forms at each temperature. The amount of the QLL depends on the thermal history of the sample; for instance, the shoulder above 380 nm is less intensive in some cases than in others, as is shown in Fig. S14, which compares emissions of two MeNp crystals that have different thermal histories despite being measured at 77 K. Regarding the cooling rate enabled by our cryostat (2 K min^{-1}), the starting temperature of 200 K delivers an excimer more conspicuous than that produced at higher initial temperatures (210 K and 220 K); the effect can be explained by a higher viscosity of the QLL at a lower temperature. The QLL on the surface may be kinetically arrested by rapid quenching (below 150 K; see Fig. S1) and released only via annealing at temperatures above approximately 190 K (Fig. S14 and Fig. S15). Such behavior is reminiscent of the kinetically trapped crystal faults that relax at higher temperatures [6]. On the other hand, the QLL becomes thicker at 200 K or even 170 K, and these observations suggest that beyond 170 K the amount of the QLL is thermodynamically controlled, increasing on QLL-free crystals but diminishing when the quenched QLL is thicker than that in the thermodynamic limit.

4.5. Consequences

The ability to excite the MeNp in various speciations by light with diverse wavelengths (up to 325 nm in crystals at 77 K, 335 nm in MeNp glass at 77 K, and 345 nm in liquid at 295 K) corresponds well to the red edge of the excitation spectra (Fig. 1, B) and can be used to selectively address the MeNp states in molecular switch-like applications [78] or multi-stimulus responsive luminescent materials [79]. For that purpose, the temperature and excitation wavelengths embody two independent input variables, combinable with diverse cooling rates to construct the logical gates; the output is the proportion of the excimer emission to that of the monomer.

In the context of environmental chemistry, the MeNp can be considered a model to form secondary organic aerosols [80]; within this domain, the distinction between the crystalline and the amorphous phases is of importance [22,81,82]. The observed bathochromic shifts of the absorption spectra in the respective condensed phases play a major role in the photodegradation [33,83–85]. In the spectral region between 317 nm (diluted solution) and 345 nm (liquid MeNp), the radiative flux in the troposphere increases substantially [86], suggesting a faster phototransformation of the MeNp in the condensed phases compared to the aqueous solutions.

5. Conclusion

Both the crystal and the glass of the MeNp show reversible spectral changes between 77 K and 150 K. We suggest that these features correspond to an increasing vibrational freedom in crystals in the ground state and in glass predominantly in the excited state.

In the glass, heating ensures transformation into a supercooled liquid, as observed at around 150 K, and the subsequent cold crystallization results in crystals of MeNp ($T_x > 165$ K). The T_g temperature is slightly higher in the sample cooled fast in liquid methane, reaching 160 K, than in the samples cooled down more slowly in liquid nitrogen at

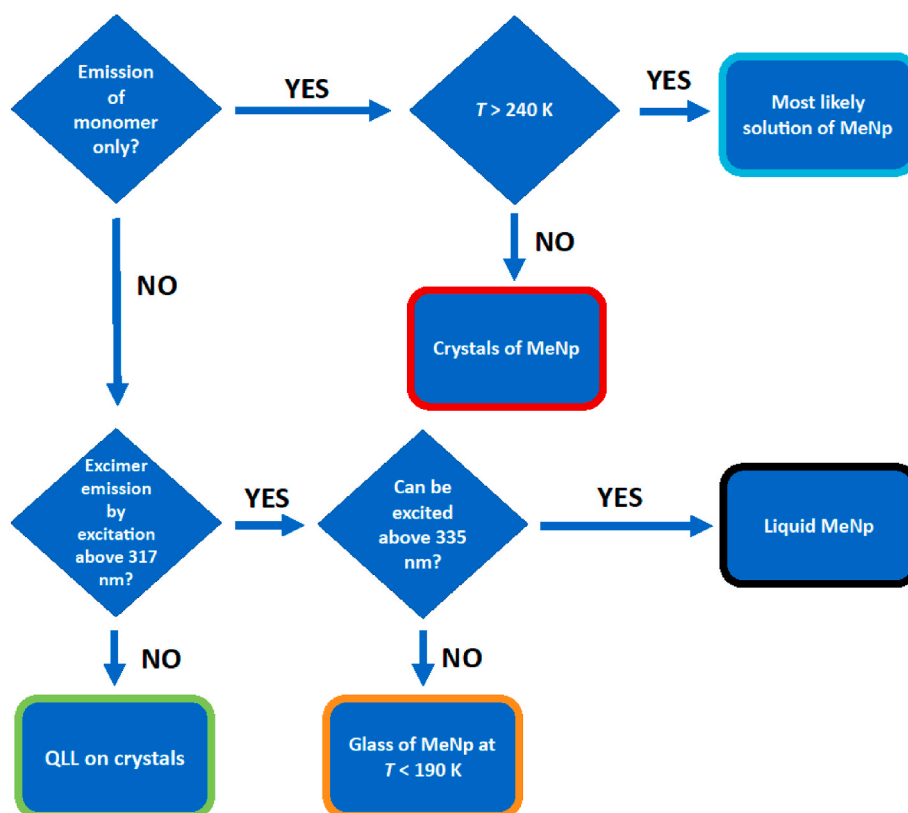
150 K; such a situation is expectable due to the higher fictive temperatures in the rapidly cooled glasses. The absence of hysteresis in the fluorescence spectra of amorphous MeNp below the T_x allows comparing the glass with the thermoplastic polymers. The crystallization is slow (presumably because of the high glass viscosity), lasting hundreds of minutes at 180 K.

Spectral features typical of crystals, such as a vibrationally resolved monomer-like emission, are reported in the slow-cooled samples (ca 2 K min^{-1}). There appears an excimeric emission superimposed on a crystal monomeric emission at temperatures above ca. 170 K; this effect is more pronounced at higher temperatures and requires tens of minutes to reach an equilibrium at 200 K. We suggest interpreting this behavior in terms of surface pre-melting (QLL). The very viscous QLL exhibits slow dynamics during the cooling, as its width stays high in the fast cooled samples, where the crystallization proceeds slowly, and remains unfinished below 150 K. The thickness of the QLL seems to be thermodynamically controlled above 170 K. The MeNp glass and the QLL embody two distinct, disordered environments, which are stable below 150 K. The excitation spectra, together with the excimeric emission, is suggestive of ground state interactions tentatively ascribed to dimers.

Combinations of the emission and the excitation spectra unambiguously characterize the state of the MeNp, as is summarized by the flowchart in Scheme 1, accompanied with the model excitation spectra in Fig. 10. The excitation and emission wavelengths, sample temperature, and thermal history all render MeNp applicable as a molecular switch. The acquired knowledge of the MeNp speciation at sub-zero temperatures will allow the compound to be employed as a molecular probe in research of the FCS in (sea) ice.

Declaration of competing interest

The authors declare that they have no known competing financial interests or personal relationships that could have appeared to influence the work reported in this paper.



Scheme 1. The flowchart to distinguish the MeNp species from the fluorescence spectra (Fig. 10).

Data availability

Data will be made available on request.

Acknowledgments

J.Z. thanks CEEPUS for the grant M – SI-1312-2122-150432 in the frame of the network “Water – a common but anomalous substance that has to be taught and studied”. Dedicated to the memory of Professor Jakob (Joggi) Wirz of the University of Basel, Switzerland.

Appendix A. Supplementary data

Supplementary data to this article can be found online at <https://doi.org/10.1016/j.jlumin.2023.119917>.

References

- [1] T. Bartels-Rausch, H.W. Jacobi, T.F. Kahan, et al., A review of air–ice chemical and physical interactions (AICI): liquids, quasi-liquids, and solids in snow, *Atmos. Chem. Phys.* 14 (3) (2014) 1587–1633, <https://doi.org/10.5194/acp-14-1587-2014>.
- [2] V.F. Petrenko, R.W. Whitworth, *Physics of Ice*, Oxford University Press, Oxford, 1999.
- [3] C.A. Colberg, B.P. Luo, H. Wernli, et al., A novel model to predict the physical state of atmospheric H₂SO₄/NH₃/H₂O aerosol particles, *Atmos. Chem. Phys.* 3 (2003) 909–924, <https://doi.org/10.5194/acp-3-909-2003>.
- [4] S.T. Martin, Phase transitions of aqueous atmospheric particles, *Chem. Rev.* 100 (9) (2000) 3403–3453, <https://doi.org/10.1021/cr990034t>.
- [5] R.S. Disselkamp, S.E. Anthony, A.J. Prenni, et al., Crystallization kinetics of nitric acid dihydrate aerosols, *J. Phys. Chem.* 100 (21) (1996) 9127–9137, <https://doi.org/10.1021/jp953608g>.
- [6] M.D. Ediger, C.A. Angell, S.R. Nagel, Supercooled liquids and glasses, *J. Phys. Chem.* 100 (31) (1996) 13200–13212, <https://doi.org/10.1021/jp953538d>.
- [7] P.G. Debenedetti, F.H. Stillinger, Supercooled liquids and the glass transition, *Nature* 410 (6825) (2001) 259–267, <https://doi.org/10.1038/35065704>.
- [8] M.Q. Jiang, M. Naderi, Y.J. Wang, et al., Thermal expansion accompanying the glass-liquid transition and crystallization, *AIP Adv.* 5 (12) (2015) 7, <https://doi.org/10.1063/1.4939216>.
- [9] F.H. Stillinger, P.G. Debenedetti, Distinguishing vibrational and structural equilibration contributions to thermal expansion, *J. Phys. Chem. B* 103 (20) (1999) 4052–4059, <https://doi.org/10.1021/jp983831o>.
- [10] Y. He, R.B. Schwarz, D. Mandrus, et al., Elastic moduli, density, and structural relaxation in bulk amorphous Zr_{41.2}Ti_{11.3}Cu_{12.5}Ni₁₀Be_{22.5} alloy, *J. Non-Cryst. Solids* 207 (1996) 602–606.
- [11] J.C. Bendert, A.K. Gangopadhyay, N.A. Mauro, et al., Volume expansion measurements in metallic liquids and their relation to fragility and glass forming ability: an energy landscape interpretation, *Phys. Rev. Lett.* 109 (18) (2012), 185901, <https://doi.org/10.1103/PhysRevLett.109.185901>.
- [12] J.C. Dyre, Colloquium: the glass transition and elastic models of glass-forming liquids, *Rev. Mod. Phys.* 78 (3) (2006) 953–972, <https://doi.org/10.1103/RevModPhys.78.953>.
- [13] F. Dominé, I. Xueref, Evaluation of depth profiling using laser resonant desorption as a method to measure diffusion coefficients in ice, *Anal. Chem.* 73 (17) (2001) 4348–4353, <https://doi.org/10.1021/ac010255a>.
- [14] O. Andersson, A. Inaba, Thermal conductivity of crystalline and amorphous ices and its implications on amorphization and glassy water, *Phys. Chem. Chem. Phys.* 7 (7) (2005) 1441–1449, <https://doi.org/10.1039/b500373c>.
- [15] A.I. Krivchikov, O. Andersson, Thermal conductivity of triphenyl phosphite's liquid, glassy, and glacial states, *J. Phys. Chem. B* 120 (10) (2016) 2845–2853, <https://doi.org/10.1021/acs.jpcc.6b00271>.
- [16] O. Andersson, G.P. Johari, Thermal conductivity of Glycerol's liquid, glass, and crystal states, glass-liquid-glass transition, and crystallization at high pressures, *J. Chem. Phys.* 144 (6) (2016) 10, <https://doi.org/10.1063/1.4941335>.
- [17] O. Andersson, Thermal conductivity of normal and deuterated water, crystalline ice, and amorphous ices, *J. Chem. Phys.* 149 (12) (2018) 8, <https://doi.org/10.1063/1.5050172>.
- [18] G.P. Johari, O. Andersson, Structural relaxation and thermal conductivity of high-pressure formed, high-density di-n-butyl phthalate glass and pressure induced departures from equilibrium state, *J. Chem. Phys.* 146 (23) (2017) 10, <https://doi.org/10.1063/1.4986063>.
- [19] M. Nachbar, D. Duft, T. Leisner, The vapor pressure of liquid and solid water phases at conditions relevant to the atmosphere, *J. Chem. Phys.* 151 (6) (2019), 064504, <https://doi.org/10.1063/1.5100364>.
- [20] S.A. Dalhatu, R. Hussin, K. Deraman, Structural and luminescence properties of Eu³⁺-doped magnesium sulfide borate glass and crystal, *Chin. J. Phys.* 54 (6) (2016) 877–882, <https://doi.org/10.1016/j.cjph.2016.10.009>.
- [21] I. Kohl, E. Mayer, A. Hallbrucker, The glassy water-cubic ice system: a comparative study by X-ray diffraction and differential scanning calorimetry, *Phys. Chem. Chem. Phys.* 2 (8) (2000) 1579–1586, <https://doi.org/10.1039/a908688i>.
- [22] B. Zobrist, C. Marcolli, D.A. Pedernera, et al., Do atmospheric aerosols form glasses? *Atmos. Chem. Phys.* 8 (17) (2008) 5221–5244, <https://doi.org/10.5194/acp-8-5221-2008>.
- [23] H. Kanno, C.A. Angell, Homogeneous nucleation and glass formation in aqueous alkali halide solutions at high pressures, *J. Phys. Chem.* 81 (26) (1977) 2639–2643, <https://doi.org/10.1021/j100541a013>.
- [24] L.J. Plaga, A. Raidt, V. Fuentes Landete, et al., Amorphous and crystalline ices studied by dielectric spectroscopy, *J. Chem. Phys.* 150 (24) (2019), 244501, <https://doi.org/10.1063/1.5100785>.
- [25] P. Gallo, K. Amann-Winkel, C.A. Angell, et al., Water: a tale of two liquids, *Chem. Rev.* 116 (13) (2016) 7463–7500, <https://doi.org/10.1021/acs.chemrev.5b00750>.
- [26] A. Karina, T. Eklund, C.M. Tonauer, et al., Infrared spectroscopy on equilibrated high-density amorphous ice, *J. Phys. Chem. Lett.* 13 (34) (2022) 7965–7971, <https://doi.org/10.1021/acs.jpclett.2c02074>.
- [27] V. Fuentes-Landete, C. Mitterdorfer, P.H. Handle, et al., Crystalline and amorphous ices. Proceedings of the international school of physics “enrico fermi”, 2015, 187: Water: Fundamentals as the Basis for Understanding the Environment and Promoting Technology: p. SIF (2015) 173–208, <https://doi.org/10.3254/978-1-61499-507-4-173>.
- [28] G. Ondrušková, L. Veselý, J. Zezula, et al., Using excimeric fluorescence to study how the cooling rate determines the behavior of naphthalenes in freeze-concentrated solutions: vitrification and crystallization, *J. Phys. Chem. B* 124 (46) (2020) 10556–10566, <https://doi.org/10.1021/acs.jpcc.0c07817>.
- [29] W. Wang, S. Ohtake, Science and art of protein formulation development, *Int. J. Pharm.* 568 (2019), 118505, <https://doi.org/10.1016/j.ijpharm.2019.118505>.
- [30] B. Bhatnagar, B. Zakharov, A. Fisyuk, et al., Protein/ice interaction: high-resolution synchrotron X-ray diffraction differentiates pharmaceutical proteins from lysozyme, *J. Phys. Chem. B* 123 (27) (2019) 5690–5699, <https://doi.org/10.1021/acs.jpcc.9b02443>.
- [31] J. Eichler, I. Kleitz, M. Bayer-Giraldi, et al., Location and distribution of micro-inclusions in the EDML and NEMM ice cores using optical microscopy and in situ Raman spectroscopy, *Cryosphere* 11 (3) (2017) 1075–1090, <https://doi.org/10.5194/1075-1075-2017>.
- [32] M. Thangswamy, P. Maheshwari, D. Dutta, et al., EPR evidence of liquid water in ice: an intrinsic property of water or a self-confinement effect? *J. Phys. Chem. A* 122 (23) (2018) 5177–5189, <https://doi.org/10.1021/acs.jpca.8b03605>.
- [33] D. Heger, P. Klan, Interactions of organic molecules at grain boundaries in ice: a solvatochromic analysis, *J. Photochem. Photobiol. Chem.* 187 (2–3) (2007) 275–284, <https://doi.org/10.1016/j.jphotochem.2006.10.012>.
- [34] D. Heger, J. Jirkovsky, P. Klan, Aggregation of methylene blue in frozen aqueous solutions studied by absorption spectroscopy, *J. Phys. Chem. A* 109 (30) (2005) 6702–6709, <https://doi.org/10.1021/jp050439j>.
- [35] D. Heger, J. Klanova, P. Klan, Enhanced protonation of cresol red in acidic aqueous solutions caused by freezing, *J. Phys. Chem. B* 110 (3) (2006) 1277–1287, <https://doi.org/10.1021/jp0553683>.
- [36] K. Imrichova, L. Veselý, T.M. Gasser, et al., Vitrification and increase of basicity in between ice Ih crystals in rapidly frozen dilute NaCl aqueous solutions, *J. Chem. Phys.* 151 (1) (2019), 014503, <https://doi.org/10.1063/1.5100852>.
- [37] L. Veselý, B. Susrisweta, D. Heger, Making good's buffers good for freezing: the acidity changes and their elimination via mixing with sodium phosphate, *Int. J. Pharm.* 593 (2021), 120128, <https://doi.org/10.1016/j.ijpharm.2020.120128>.
- [38] R. Kania, J.K.E. Malongwe, D. Nachtigalová, et al., Spectroscopic properties of benzene at the air–ice interface: a combined experimental–computational approach, *J. Phys. Chem.* 118 (35) (2014) 7535–7547, <https://doi.org/10.1021/jp501094n>.
- [39] J. Krausko, J.K.E. Malongwe, G. Bičanová, et al., Spectroscopic properties of naphthalene on the surface of ice grains revisited: a combined experimental–computational approach, *J. Phys. Chem.* 119 (32) (2015) 8565–8578, <https://doi.org/10.1021/acs.jpca.5b00941>.
- [40] G. Ondrušková, J. Krausko, J.N. Stern, et al., Distinct speciation of naphthalene vapor deposited on ice surfaces at 253 or 77 K: formation of submicrometer-sized crystals or an amorphous layer, *J. Phys. Chem. C* 122 (22) (2018) 11945–11953, <https://doi.org/10.1021/acs.jpcc.8b03972>.
- [41] P. Klan, J. Wirz, *Photochemistry of Organic Compounds: from Concepts to Practice*, first ed., John Wiley & Sons Ltd, Chichester, 2009, p. 584.
- [42] N. Mataga, M. Tomura, H. Nishimura, Fluorescence decay times of naphthalene and naphthalene excimers, *Mol. Phys.* 9 (4) (1965) 367–375, <https://doi.org/10.1080/00268976500100501>.
- [43] J.P. McCullough, H.L. Finke, J.F. Messerly, et al., The low-temperature thermodynamic properties of naphthalene, 1-methylnaphthalene, 2-methylnaphthalene, 1,2,3,4-tetrahydronaphthalene, trans-decahydronaphthalene and cis-decahydronaphthalene, *J. Phys. Chem.* 61 (8) (1957) 1105–1116, <https://doi.org/10.1021/j150554a016>.
- [44] C. Yokoyama, T. Ebina, S. Takahashi, Melting temperatures of several polycyclic and heteropolycyclic aromatic compounds under high pressures, *Fluid Phase Equil.* 84 (1993) 207–223, [https://doi.org/10.1016/0378-3812\(93\)85124-5](https://doi.org/10.1016/0378-3812(93)85124-5).
- [45] L. Antonov, Drawbacks of the present standards for processing absorption spectra recorded linearly as a function of wavelength, *Trac-Trend. Anal. Chem.* 16 (9) (1997) 536–543.
- [46] V. Petrov, L. Antonov, H. Ehara, et al., Step by step filter based program for calculations of highly informative derivative curves, *Comput. Chem.* 24 (5) (2000) 561–569.
- [47] J. Bachler, P.H. Handle, N. Giovambattista, et al., Glass polymorphism and liquid-liquid phase transition in aqueous solutions: experiments and computer simulations, *Phys. Chem. Chem. Phys.* 21 (42) (2019) 23238–23268, <https://doi.org/10.1039/c9cp02953b>.

- [48] Y. Tsuboi, K. Irie, H. Miyasaka, et al., Nonlinear photophysics and ablation of liquid naphthalene derivatives: fluence-dependence of luminescence spectra upon 248 nm laser excitation, *J. Phys. Chem. A* 107 (17) (2003) 3017–3023, <https://doi.org/10.1021/jp021615g>.
- [49] H.C. Wolf, Zum spektroskopischen VERHALTEN der METHYLDERIVATE des naphthalins und zur frage der spektroskopischen ANALYSIERBARKEIT STELLUNGSISSOMERERER AROMATISCHER KOHLENWASSERSTOFFE, *Zeitschrift Fur Naturforschung Part a-Astrophysik Physik Und Physikalische Chemie* 10 (4) (1955) 270–278.
- [50] T. Kawakubo, On the emission of naphthalene and some of its derivatives in the crystalline state, *Mol. Cryst. Liq. Cryst.* 16 (4) (1972) 333–353, <https://doi.org/10.1080/15421407208082795>.
- [51] D. Heger, D. Nachtigallova, F. Surman, et al., Self-organization of 1-methylnaphthalene on the surface of artificial snow grains: a combined experimental-computational approach, *J. Phys. Chem. A* 115 (41) (2011) 11412–11422, <https://doi.org/10.1021/jp205627a>.
- [52] A.L.L. East, E.C. Lim, Naphthalene dimer: electronic states, excimers, and triplet decay, *J. Chem. Phys.* 113 (20) (2000) 8981–8994, <https://doi.org/10.1063/1.1319345>.
- [53] H. Drozdowski, Local structure and molecular correlations in liquid 1-methylnaphthalene at 293 K, *Chem. Phys. Lett.* 351 (2002) 53–60, [https://doi.org/10.1016/S0009-2614\(01\)01364-1](https://doi.org/10.1016/S0009-2614(01)01364-1).
- [54] T.F. Headen, C.A. Howard, N.T. Skipper, et al., Structure of $\pi-\pi$ interactions in aromatic liquids, *J. Am. Chem. Soc.* 132 (16) (2010) 5735–5742, <https://doi.org/10.1021/ja909084e>.
- [55] E.S. Iyer, A. Sadybekov, O. Lioubashevski, et al., Rewriting the story of excimer formation in liquid benzene, *J. Phys. Chem. A* 121 (9) (2017) 1962–1975, <https://doi.org/10.1021/acs.jpca.7b01070>.
- [56] J.G. Dash, A.W. Rempel, J.S. Wettlaufer, The physics of premelted ice and its geophysical consequences, *Rev. Mod. Phys.* 78 (3) (2006) 695–741, <https://doi.org/10.1103/RevModPhys.78.695>.
- [57] X.P. Wang, B. Li, X.L. Xu, et al., Surface roughening, premelting and melting of monolayer and bilayer crystals, *Soft Matter* 17 (3) (2021) 688–693, <https://doi.org/10.1039/d0sm01589j>.
- [58] B. Li, F. Wang, D. Zhou, et al., Modes of surface premelting in colloidal crystals composed of attractive particles, *Nature* 531 (7595) (2016) 485–488, <https://doi.org/10.1038/nature16987>.
- [59] Y. Djilkaev, E. Ruckenstein, A kinetic model for the premelting of a crystalline structure, *Phys. Stat. Mech. Appl.* 387 (1) (2008) 134–144, <https://doi.org/10.1016/j.physa.2007.08.022>.
- [60] M.I. Faraday, Note on Regelation, vol. 10, *Proceedings of the Royal Society of London*, 1860, pp. 440–450, <https://doi.org/10.1098/rspl.1859.0082>.
- [61] V.F. McNeill, T. Loerting, F.M. Geiger, et al., Hydrogen chloride-induced surface disordering on ice, *Proc. Natl. Acad. Sci. USA* 103 (25) (2006) 9422–9427, <https://doi.org/10.1073/pnas.0603494103>.
- [62] J.W.M. Frenken, J.F.v.d. Veen, Observation of surface melting, *Phys. Rev. Lett.* 54 (2) (1985) 134–137, <https://doi.org/10.1103/PhysRevLett.54.134>.
- [63] D.M. Zhu, J.G. Dash, Surface melting and roughening of adsorbed argon films, *Phys. Rev. Lett.* 57 (23) (1986) 2959–2962, <https://doi.org/10.1103/PhysRevLett.57.2959>.
- [64] H.N. Smith, H.H. Heady, Identification of frozen liquid samples with X-ray diffractometer, *Anal. Chem.* 27 (6) (1955) 883–888, <https://doi.org/10.1021/ac60102a005>.
- [65] J.M. Robertson, W.H. Bragg, The crystalline structure of naphthalene. A quantitative X-ray investigation, *Proc. R. Soc. Lond. - Ser. A Contain. Pap. a Math. Phys. Character* 142 (847) (1933) 674–688, <https://doi.org/10.1098/rspa.1933.0197>.
- [66] G.E. Berkovic, Z. Ludmer, Crystal excimer fluorescence from substituted naphthalenes, *J. Lumin.* 26 (4) (1982) 463–467, [https://doi.org/10.1016/0022-2313\(82\)90074-6](https://doi.org/10.1016/0022-2313(82)90074-6).
- [67] A. Meresse, N.B. Chanh, J. Housty, et al., Characterization of the polymorphism of 2-METHYLNAPHTHALENE, *J. Appl. Crystallogr.* 16 (AUG) (1983) 370–373, <https://doi.org/10.1107/s002188988301064x>.
- [68] M. Adda-Bedia, S. Kumar, F. Lechenault, et al., Inverse Leidenfrost effect: levitating drops on liquid nitrogen, *Langmuir* 32 (17) (2016) 4179–4188, <https://doi.org/10.1021/acs.langmuir.6b00574>.
- [69] H.K. Feng, Y. Xu, T.T. Yang, Study on Leidenfrost effect of cryoprotectant droplets on liquid nitrogen with IR imaging technology and non-isothermal crystallization kinetics model, *Int. J. Heat Mass Tran.* 127 (2018) 413–421, <https://doi.org/10.1016/j.ijheatmasstransfer.2018.08.001>.
- [70] Y.S. Song, D. Adler, F. Xu, et al., Vitrification and levitation of a liquid droplet on liquid nitrogen, *Proc. Natl. Acad. Sci. USA* 107 (10) (2010) 4596–4600, <https://doi.org/10.1073/pnas.0914059107>.
- [71] C.T. Moynihan, A.J. Easteal, M.A. Debolt, et al., Dependence of fictive temperature of glass on cooling rate, *J. Am. Ceram. Soc.* 59 (1–2) (1976) 12–16, <https://doi.org/10.1111/j.1151-2916.1976.tb09376.x>.
- [72] S.Y. Gao, S.L. Simon, Measurement of the limiting fictive temperature over five decades of cooling and heating rates, *Thermochim. Acta* 603 (2015) 123–127, <https://doi.org/10.1016/j.tca.2014.08.019>.
- [73] Y.Z. Yue, R. von der Ohe, S.L. Jensen, Fictive temperature, cooling rate, and viscosity of glasses, *J. Chem. Phys.* 120 (17) (2004) 8053–8059, <https://doi.org/10.1063/1.1689951>.
- [74] P.G. Debenedetti, *Metastable Liquids : Concepts and Principles*, Princeton University Press, Princeton, 1996.
- [75] U. Retzer, H. Ulrich, F.J. Bauer, et al., UV absorption cross sections of vaporized 1-methylnaphthalene at elevated temperatures, *Appl. Phys. B Laser Opt.* 126 (3) (2020) 6, <https://doi.org/10.1007/s00340-020-7400-z>.
- [76] S.R. Gardner, L.M. Selby, R.K. Teranishi, et al., Temperature dependent excimer luminescence of naphthalenes on α -alumina, *J. Lumin.* 134 (2013) 657–664, <https://doi.org/10.1016/j.jlumin.2012.07.013>.
- [77] H. Nakayama, T. Hosokawa, K. Ishii, Fluorescence spectra and energy transfer in amorphous naphthalene, *Chem. Phys. Lett.* 289 (3–4) (1998) 275–280, [https://doi.org/10.1016/S0009-2614\(98\)00423-0](https://doi.org/10.1016/S0009-2614(98)00423-0).
- [78] A. Credi, Molecules that make decisions, *Angew. Chem. Int. Ed. Engl.* 46 (29) (2007) 5472–5475, <https://doi.org/10.1002/anie.200700879>.
- [79] Z.F. Liu, L. Zeng, L.Y. Niu, et al., Rotors tailoring molecular stacking for constructing multi-stimuli-responsive luminescent materials, *Chem. Commun.* 59 (17) (2023) 2453–2456, <https://doi.org/10.1039/d2cc06847h>.
- [80] X. Wang, R. Gemayel, V.J. Baboornian, et al., Naphthalene-derived secondary organic aerosols interfacial photosensitizing properties, *Geophys. Res. Lett.* 48 (13) (2021), <https://doi.org/10.1029/2021gl093465>.
- [81] P.A. Alpert, J. Dou, P. Corral Arroyo, et al., Photolytic radical persistence due to anoxia in viscous aerosol particles, *Nat. Commun.* 12 (1) (2021) 1769, <https://doi.org/10.1038/s41467-021-21913-x>.
- [82] Y. Cheng, H. Su, T. Koop, et al., Size dependence of phase transitions in aerosol nanoparticles, *Nat. Commun.* 6 (1) (2015), <https://doi.org/10.1038/ncomms6923>.
- [83] J. Literak, P. Klan, D. Heger, et al., Photochemistry of alkyl aryl ketones on alumina, silica-gel and water ice surfaces, *J. Photochem. Photobiol. Chem.* 154 (2–3) (2003) 155–159.
- [84] M. Mekic, S. Gligorovski, Ionic Strength Effects on Heterogeneous and Multiphase Chemistry: Clouds versus Aerosol Particles, vol. 244, *Atmospheric Environment*, 2021, <https://doi.org/10.1016/j.atmosenv.2020.117911>.
- [85] F.C. Bononi, Z. Chen, D. Rocca, et al., Bathochromic shift in the UV-visible absorption spectra of phenols at ice surfaces: insights from first-principles calculations, *J. Phys. Chem. A* (2020), <https://doi.org/10.1021/acs.jpca.0c07038>.
- [86] S. Madronich, S. Flocke, The role of solar radiation in atmospheric chemistry, in: P. Boule (Ed.), *Environmental Photochemistry*, Springer Berlin Heidelberg, Berlin, Heidelberg, 1999, pp. 1–26, https://doi.org/10.1007/978-3-540-69044-3_1.